Ionization and fragmentation of polycyclic aromatic hydrocarbon clusters in collisions with keV ions

H. A. B. Johansson,[1] H. Zettergren,[1] A. I. S. Holm,[1] F. Seitz,[1] H. T. Schmidt,[1] P. Rousseau,[2] A. Ławicki,[2] M. Capron,[2] A. Domaracka,[2] E. Lattouf,[2] S. Maclot,[2] R. Maisonny,[2] B. Manil,[3] J.-Y. Chesnel,[2] L. Adoui,[2] B. A. Huber,[2] and H. Cederquist[1]

[1]*Department of Physics, Stockholm University, SE-106 91, Stockholm, Sweden*

[2]*CIMAP, UMR 6252, CEA/CNRS/ENSICAEN/Université de Caen Basse-Normandie, Boulevard Henri Becquerel, BP5133, F-14070 Caen Cedex 5, France*

[3]*Laboratoire de Physique des Laser, CNRS, UMR 7538, Institut Galilée, Université Paris 13, F-93430, Villetaneuse, France*

(Received 21 July 2011; published 10 October 2011)

We report on an experimental study of the ionization and fragmentation of clusters of k polycyclic aromatic hydrocarbon (PAH) molecules using anthracene, $C_{14}H_{10}$, or coronene, $C_{24}H_{12}$. These PAH clusters are moderately charged and strongly heated in small impact parameter collisions with 22.5-keV He^{2+} ions, after which they mostly decay in long monomer evaporation sequences with singly charged and comparatively cold monomers as dominating end products. We describe a simple cluster evaporation model and estimate the number of PAH molecules in the clusters that have to be hit by He^{2+} projectiles for such complete cluster evaporations to occur. Highly charged and initially cold clusters are efficiently formed in collisions with 360-keV Xe^{20+} ions, leading to cluster Coulomb explosions and several hot charged fragments, which again predominantly yield singly charged, but much hotter, monomer ions than the He^{2+} collisions. We present a simple formula, based on density-functional-theory calculations, for the ionization energy sequences as functions of coronene cluster size, rationalized in terms of the classic electrostatic expression for the ionization of a charged conducting object. Our analysis indicates that multiple electron removal by highly charged ions from a cluster of PAH molecules rapidly may become more important than single ionization as the cluster size k increases and that this is the main reason for the unexpectedly strong heating in these types of collisions.

DOI: 10.1103/PhysRevA.84.043201 PACS number(s): 36.40.Qv, 33.15.Ry, 36.40.Wa

I. INTRODUCTION

Polycyclic aromatic hydrocarbons (PAHs) are a group of molecules that has attracted much attention in recent years. As pollutants, PAHs have been studied to learn about their growth and formation mechanisms [1] as well as their influence on the environment [2] and on human health [3]. In the interstellar medium the bending and stretching modes of individual PAH molecules are generally believed to be the sources of distinct infrared emission features in the ∼3–20-μm wavelength region observed in both galactic and extragalactic sources [4].

Clusters of PAHs are studied as soot precursors [5] but are also interesting as potential candidates in electronic nanodevices [6]. In the astronomical context, PAH clusters have been suggested to be the cause of the broader emission bands at 7.8 and 11.4 μm, as well as the strong continuum emission in the 5–25-μm range, observed in, e.g., photodissociation regions [7,8]. These PAH clusters have been suggested to contain at least 400 carbon atoms [7], and it is of interest to investigate how such clusters will react when exposed to ionizing radiation, such as photons or stellar wind ions. From a more fundamental perspective, collisions between keV ions and PAH clusters may be used to shed light on stabilities, energy flow processes, and charge mobility within weakly bound molecular clusters.

Anthracene, $C_{14}H_{10}$, and coronene, $C_{24}H_{12}$, are examples of two PAH molecules. They differ in that anthracene is a catacondensed PAH with three benzene-like rings in a chainlike configuration, while coronene is symmetric and centrally condensed (pericondensed) with seven benzene-like rings in a plane. The fragmentation behaviors of both these molecules have been studied through UV photodissociation [9–17], collision-induced dissociation in which the PAH ions collide with neutral targets [18,19], and fragmentation of initially neutral PAHs induced by keV collisions with atomic ions [20–22]. These experiments have established that the dissociation channels with the lowest activation energies are the losses of H, H_2, and C_2H_2, which all lie in the 4.3–4.6-eV range for, e.g., the anthracene cation [13]. For neutral coronene and its cation, comparisons with calculated adiabatic dissociation energies suggest a similar energy range for the H losses, while C_2H_2 loss requires substantially more energy [23]. First ionization energies (IEs) have been measured to be 7.4 eV for anthracene [24,25] and 7.2 eV for coronene [26–29], while the second IEs have been found to be 11.2–11.3 eV for coronene [28,29] and 12.1 eV for anthracene [27]. These values are in good agreement with theoretical results [23,28,30].

Theoretical work on anthracene and coronene *clusters* have this far mainly been aimed at studies of geometrical structures and cluster binding energies. Such calculations are difficult since they concern large numbers of degrees of freedom, shallow potential energy surfaces, and abundances of local energy minima interconnected by large structural rearrangements. Calculations of anthracene cluster geometries and binding energies are particularly demanding with significant complexity even for the smaller cluster sizes [31–34]. Stacked geometries, with parallel molecular planes and the long axes of the molecules aligned or perpendicular, or geometries with tilted molecular planes have been proposed for the neutral anthracene dimer, trimer, and tetramer [33,34]. For larger neutral anthracene clusters a herringbone configuration, found in anthracene crystals, may be favorable [34,35]. Typical binding energies are ∼0.2–0.4 eV [33,36,37] for the neutral anthracene dimer and ∼0.6–0.8 eV for the ionized dimer [33].

The neutral coronene dimer has been extensively studied with quantum chemical methods, indicating that structures

with parallel coronene planes but with slightly displaced or twisted configurations have the largest binding energies at ∼0.8–1.0 eV [38–42]. Single stacked structures seem to be favored for clusters consisting of up to eight coronene molecules [43]. For ionized coronene clusters it has been reported that the dissociation energies for evaporation of a neutral molecule decrease with increasing cluster size [44].

Previous experimental studies of ionization and fragmentation of anthracene [21,34,45,46] and coronene [47,48] clusters have mainly been based on photoexcitation methods. From the first experiment on *ion* collisions on PAH *clusters* it was reported that (i) small- and medium-sized anthracene clusters always fragment even when they are only singly ionized in collisions with He^+ ions, (ii) charge and excitation energy is redistributed within the cluster prior to fragmentation, and (iii) very strong intermolecular heating is induced in cluster fragmentation following collisions with Xe^{20+} ions [21]. Here we report results on the ionization and fragmentation of clusters of the substantially larger PAH molecule coronene following collisions with 22.5-keV He^{2+} and 360-keV Xe^{20+} ions as well as results for He^{2+} ions colliding with anthracene clusters and monomers. The He^{2+} results will be discussed in view of a simple evaporation model, which shows that collisionally heated PAH clusters in low-charge states mostly decay in long series of monomer evaporations that often leave comparatively cold, singly charged, intact PAH monomers as end products. In the discussions of the ionization and fragmentation results for the Xe^{20+} projectiles we will use a simple formula, which is based on density-functional-theory (DFT) calculations, for single and multiple IEs for coronene clusters of various sizes. We will argue that multiple ionization may dominate strongly over single ionization, especially for large PAH clusters. A strong propensity for multiple ionizations leading to subsequent heating of the fragmentation products by Coulomb explosions, and thus to internally heated singly charged monomers, which often decay further, may well be the key to understanding the present results for PAH clusters interacting with highly charged ions.

II. EXPERIMENT

The experiment was carried out at the Accélérateurs pour les Recherches Interdisciplinaires avec les Ions de Basse Energie (ARIBE) facility of Grand Accelerateur National d'Ions Lourds (GANIL) in Caen, France. A detailed description of the experimental setup is given in Ref. [49]. In brief, beams of 22.5-keV $^3He^{2+}$ and 360-keV $^{129}Xe^{20+}$ ions were generated using an electron cyclotron resonance ion source. The ion beams were separated using a bending magnet and chopped into 1-μs-long pulses, with a repetition rate of 1.5 kHz.

An effusive jet of anthracene *monomers* was produced through evaporation at 60 °C of anthracene powder (⩾99.0% purity, from Fluka) in an oven. A second oven, heated to 120 °C, was used to efficiently produce anthracene *clusters* by cooling the gas jet with a flow of liquid-nitrogen-cooled helium. The monomer contribution in the cluster beam is estimated to be less than 1% [21]. Coronene *monomers* were produced by evaporation of coronene powder (97% purity, from Sigma-Aldrich) at 250 °C. The same temperature was used in the second oven inside the liquid-nitrogen-cooled helium gas container to produce coronene *clusters*.

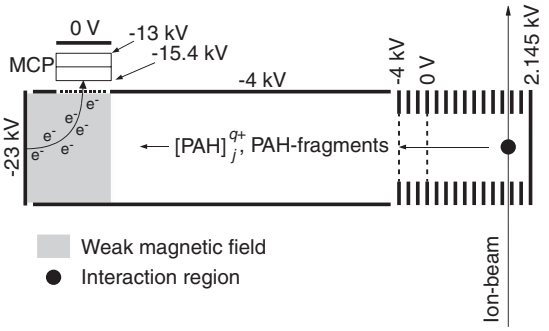

FIG. 1. Schematic of the time-of-flight mass spectrometer used in the experiment. The ion beams, 22.5-keV He^{2+} and 360-keV Xe^{20+}, were pulsed in 1-μs-long pulses. The extraction field was switched on 0.1 μs after the passage of the beam pulse (see text).

The gas jets were crossed with the $^3He^{2+}$ or $^{129}Xe^{20+}$ ion beams in the extraction region of a modified linear Wiley-McLaren time-of-flight mass spectrometer [50]. A schematic is shown in Fig. 1. Positively charged products from the interactions were extracted ∼0.1 μs after ion pulse passage with the extraction voltages switched on for ∼30 μs. The products were recorded on a Daly-type detector [51]. The weak magnetic field indicated in Fig. 1 was used to guide secondary electrons to the microchannel-plate (MCP) detector. Typical residual gas pressures in the experimental region were in the range of 2–5 $\times 10^{-9}$ mbars.

III. RESULTS AND DISCUSSIONS FOR He^{2+} PROJECTILES

A. Anthracene monomer and cluster targets

In Fig. 2 we show the mass-to-charge spectra due to 22.5-keV He^{2+} collisions with anthracene monomer targets and with anthracene cluster targets. In the top panel the two spectra are overlayed and normalized to the height of the $C_{14}H_{10}^+$ peak, which is the main feature in both spectra. Immediately to the right of the $C_{14}H_{10}^+$ peak (monomer target, gray curve) there are two smaller peaks corresponding to ^{13}C isotopes in the anthracene molecules, and to the left there are small features due to losses of up to four hydrogen atoms. The anthracene dication peak with associated hydrogen loss peaks is rather prominent in the monomer target spectrum. For both the anthracene monocation and dication there are features representing losses of C_2H_x, with $x = 2$, 3, and 4.

When comparing the monomer target and cluster target results in Fig. 2 we note the following: (i) There are many fewer small fragments in the cluster target case, where the overall probability for fragments below the $C_{14}H_{10}$ mass is $(10 \pm 1)\%$ compared to $(57 \pm 1)\%$ in the case of monomer targets. (ii) The $C_{14}H_{10}^+$ peak and the associated C_2H_x loss peaks are much broader in the cluster target spectrum than in the monomer target spectrum. This broadening is typical for processes associated with kinetic energy releases (KERs), and thus these peaks are products of cluster fragmentation processes in the cluster target case.

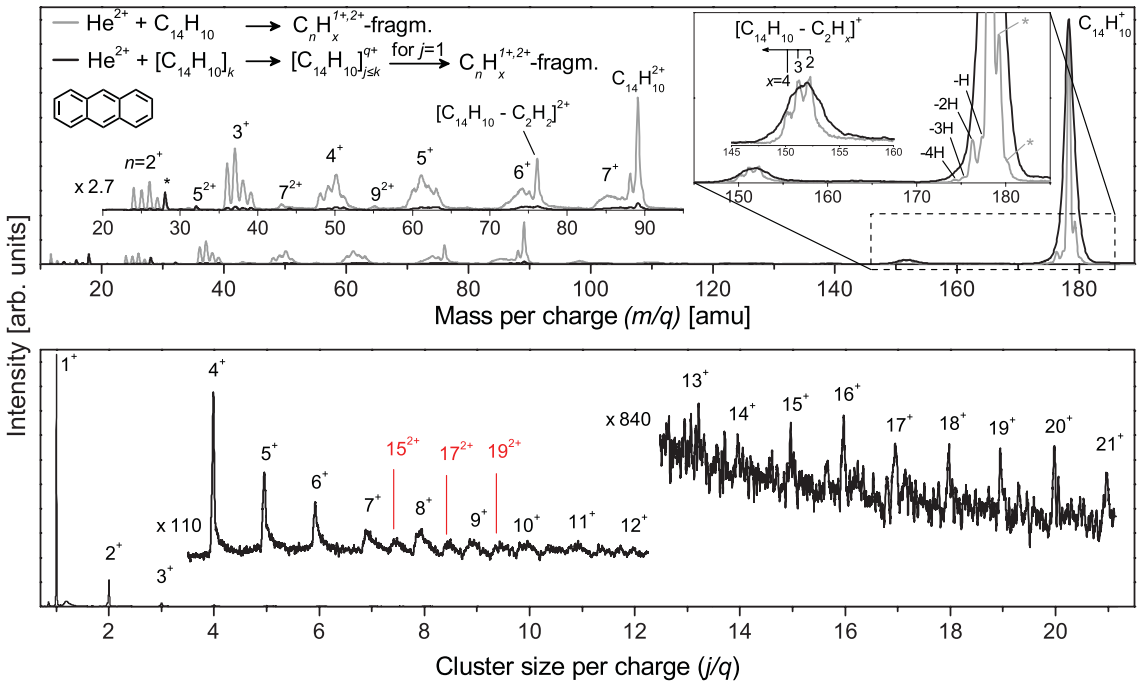

FIG. 2. (Color online) (top) Mass-to-charge spectra due to the ionization and fragmentation of the anthracene monomer target (gray curve) and the anthracene cluster target (black curve) following collisions with 22.5-keV He^{2+} ions. The anthracene molecular structure is shown in the left inset, and the two spectra are normalized to the maximum heights of the $C_{14}H_{10}^{+}$ peaks. The middle inset shows enlarged views of the regions containing charged fragments, $C_nH_x^{1+,2+}$, for $n \leqslant 7$, and the intact anthracene dication, $C_{14}H_{10}^{2+}$, with associated C_2H_2 loss channel. These peaks are clearly visible only with the monomer target (gray curve). The asterisk marks N_2^+ from the residual gas. The right inset shows enlarged views of the $C_{14}H_{10}^{+}$ peaks with their associated H losses and C_2H_x losses. Here the asterisks mark isotope peaks. (bottom) Cluster size-to-charge spectrum for He^{2+} on anthracene clusters with enlarged views for $4 \leqslant j \leqslant 12$ and for $j \geqslant 13$. Also marked are cluster dications with sizes $j \leqslant k$ (see text).

The distribution of $C_nH_x^{+}$ fragment intensities in the monomer target spectrum is mainly due to interactions at shorter distances where larger amounts of thermal energies are transferred to the anthracene molecules [21]. Postma *et al.* [20] showed that electronic stopping is the dominant heating process for single- and multiple-electron removal by keV He^{2+} ions colliding with anthracene monomers. From their calculated electronic stopping results for 8-, 20-, and 30-keV $^4He^{2+}$ collisions [20], we estimate that our target excitation energies for 22.5-keV $^3He^{2+}$ collisions typically are ~40 eV.

For the anthracene *cluster* target the doubly charged $C_nH_x^{2+}$ fragment intensities are greatly reduced in comparison to the monomer target, and thermally driven processes dominate the fragment distribution below the $C_{14}H_{10}$ mass also for the cluster target. This is most likely related to a redistribution of charge within the cluster prior to fragmentation, as has also been observed with He^{+} projectiles [21]. The strong decrease in fragmentation probability for the individual $C_{14}H_{10}^{+}$ units (spectrum below $C_{14}H_{10}$ mass) is due to a redistribution of excitation energy on several molecular building blocks in the cluster [21]. This is further supported by the fact that the dominant monomer fragment in the cluster target spectrum is the loss of C_2H_x units: C_2H_2 loss has the lowest activation energy following hydrogen loss [13]. A series of unresolved hydrogen losses most likely also contribute to the left-side wing of the broadened $C_{14}H_{10}^{+}$ peak.

The bottom panel in Fig. 2 shows the spectrum above the $C_{14}H_{10}$ mass for the anthracene cluster target. Here we detect singly charged anthracene clusters $[C_{14}H_{10}]_j^{+}$, with $j = 1$–21, and doubly charged clusters with $15 \leqslant j \leqslant 19$. Larger cluster dications may be produced as well but are not clearly resolved in the spectrum. The intensity distribution as a function of j does not follow the typical lognormal distribution [52] for cluster formation processes in cluster sources. Instead, there is a strong dominance of monomers (86% of the total intensity of clusters with $1 \leqslant j \leqslant k$ is in the $j = 1$ peak) with large KERs and a very strong decrease in cluster intensity as a function of product cluster size j. For $j \leqslant 7$, the peaks are broad with widths several times larger than what would be expected for clusters that remain intact following ionization [21]. The peaks in this region also have right-hand tails due to (delayed) evaporation during extraction on the microsecond time scale [21]. For $8 \leqslant j \leqslant 13$, the peaks are still broader due to even stronger contributions from delayed evaporation processes. Doubly charged clusters appear at $j = 15$ with similar tails. For $j \geqslant 14$, the peaks become more narrow for the singly charged clusters and do not have prominent tails, indicating that they result from fewer evaporation steps and that delayed processes are less important here.

B. Coronene monomer and cluster targets

In Fig. 3 we show the mass-to-charge spectra for 22.5-keV He^{2+} ions in collisions with coronene monomer targets and coronene cluster targets. In the top panel we compare these two sets of data, around and below the $C_{24}H_{12}$ mass. Again

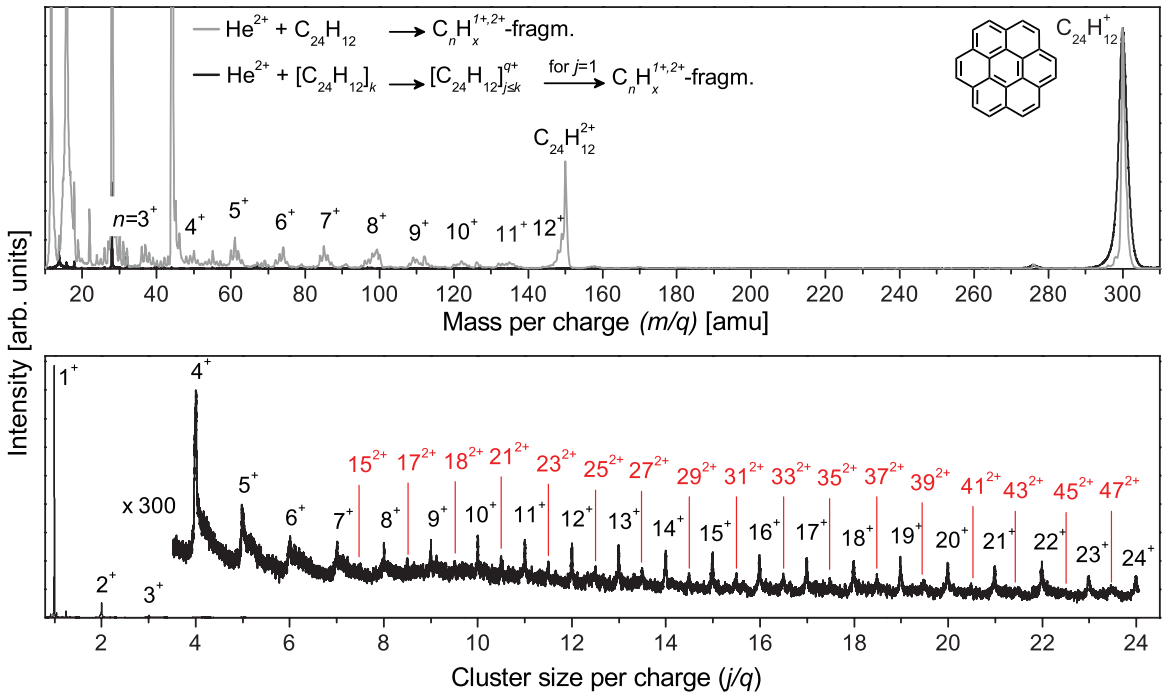

FIG. 3. (Color online) (top) Mass-to-charge spectra due to the ionization and fragmentation of the coronene monomer target (gray curve) and the coronene cluster target (black curve) following collisions with 22.5-keV He^{2+} ions. The coronene molecular structure is shown in the inset, and the two spectra are normalized to the maximum heights of the $C_{24}H_{12}^{+}$ peaks. The high-intensity peaks for $m/q < 50$ are due to ionization of the residual gas (primarily N_2 and CO_2). (bottom) Cluster size-to-charge spectrum for He^{2+} on coronene clusters with an enlarged view for $j \geqslant 4$.

we find much less fragmentation in the cluster target case, $(3 \pm 1)\%$, compared to the monomer target case, $(58 \pm 1)\%$, similar to what was found for the anthracene comparison. Doubly charged fragments are present in the spectrum for the monomer target but absent for the cluster target. The $C_{24}H_{12}^{+}$ peak in the cluster target spectrum is significantly broadened in comparison to the corresponding peak in the monomer target.

The fragments above the $C_{24}H_{12}$ mass in the coronene cluster target spectrum are shown in the bottom panel of Fig. 3. As with the anthracene clusters the spectrum is strongly dominated by the monomer peak (89% of the total intensity of clusters with $1 \leqslant j \leqslant k$ is in the $j = 1$ peak) and exhibits sharply decreasing product cluster intensities with increasing j. We observe peak tails associated with delayed fragmentation processes up to at least $j = 7$. Doubly charged clusters appear at $j = 15$, and the largest doubly charged cluster size shown here is $j = 47$. The fragmentation behavior is similar to that for the anthracene cluster target and again does not reflect the lognormal distribution expected for a cluster source. Instead, it is strongly shifted toward smaller j and in particular to the $C_{24}H_{12}^{+}$ peak ($j = 1$). We thus conclude that a large majority of all coronene (or anthracene) clusters fragment promptly following collisions with He^{2+} ions.

C. Evaporation model

Schmidt *et al.* [48] investigated the behavior of coronene clusters excited by UV-laser radiation. By describing the system as an evaporative ensemble, they concluded that a coronene cluster hot enough to evaporate one monomer unit on the 10-μs time scale also has sufficient energy for long evaporation sequences [48]. The reason for this is that only very minor parts of the internal energy are converted to kinetic energy when a single monomer unit is emitted and that the dissociation energy is small compared to the total excitation energy. The reaction products will thus have essentially the same internal energy per molecule, i.e., almost the same internal temperature, following each step of evaporation.

Following a similar approach as Schmidt *et al.* [48], we have constructed an evaporation model for internally hot coronene or anthracene clusters. The model assumes sequential evaporation of neutral monomer units from clusters in thermal equilibrium. The rate of evaporation Γ follows an Arrhenius-type equation,

$$\Gamma = A \exp(-E_d/k_B T), \tag{1}$$

where A is the preexponential factor (here set to 10^{15} s^{-1}), k_B is the Boltzmann constant, T is the temperature, and E_d is the $[PAH]_k^{q+} \rightarrow [PAH]_{k-1}^{q+} + PAH$ dissociation energy. For singly charged coronene clusters we have used calculated dissociation energies from Rapacioli and Spiegelman [44], who found them to decrease from 1.3 eV for the dimer to 0.9 eV for the octamer, approaching an asymptotic value of 0.8 eV for larger cluster sizes. The latter is the same value as for large neutral coronene clusters [44]. For anthracene we have scaled these dissociation energies by the ratio of the number of benzene rings in each molecule, i.e., by a factor of 3/7. This scaling reproduces the binding energies for the singly ionized anthracene dimer, and for larger singly charged clusters the binding energy per molecule approaches the binding energy of

the neutral dimer [33,36,37]. The latter is expected for larger cluster sizes, where the charge distribution has a maximum close to the center of the cluster [44].

In the classical high-temperature limit the relation between the cluster temperature T and the total vibrational energy $E_{\rm tot}^{\rm vib}$ for a cluster of k molecules is given by

$$E_{\rm tot}^{\rm vib} = (3kN - 6)k_BT = 3kNk_BT - 6k_BT, \qquad (2)$$

where N is the number of atoms in the individual molecules. When the total number of atoms in the clusters kN is large, the second term in Eq. (2) may be neglected, and $E_{\rm tot}^{\rm vib}$ approaches the bulk value where the total vibrational energy per molecule is $E_{\rm tot}^{\rm vib}/k = 3Nk_BT$. For an isolated molecule the vibrational energy is $(3N - 6)k_BT$, and thus the intermolecular energy per molecule in the cluster is close to $6k_BT$ for high T. This means that the intramolecular vibrational energy per molecule is $[(3N - 6)/3N] \times E_{\rm tot}^{\rm vib}/k$. For large molecular building blocks, with many degrees of freedom, the fractions of the energy stored within the individual molecules are, for high T, $(24 \times 3 - 6)/(24 \times 3) = 91.7\%$ and $(36 \times 3 - 6)/(36 \times 3) = 94.4\%$ for anthracene ($N = 24$) and for coronene ($N = 36$) clusters, respectively.

Here we take effects of finite temperatures into account by calculating the average excitation energies of the vibrational modes of the individual molecules in the harmonic approximation, $\hbar\omega_i/[\exp(\hbar\omega_i/k_BT) - 1]$ ($\hbar$ is the reduced Planck constant). We calculate the frequencies ω_i of the ith vibrational modes by means of DFT at the B3LYP/6-311++G(2d,p) level with the use of the GAUSSIAN09 program suite [53] and scale them by a factor of 0.9679 [54]. By summing over the $3N - 6$ intramolecular modes and by approximating the much smaller contribution to the total vibrational energy per molecule in the cluster due to *inter*molecular vibrations by $6k_BT$, we get

$$\frac{E_{\rm tot}^{\rm vib}(k)}{k} = \sum_{i=1}^{3N-6} \frac{\hbar\omega_i}{\exp(\hbar\omega_i/k_BT) - 1} + 6k_BT. \qquad (3)$$

For a given $E_{\rm tot}^{\rm vib}(k)/k$, the temperature T, and thus the evaporation rate Γ [Eq. (1)], may be deduced. This first step of evaporation lowers the temperature in relation to that of the parent cluster $[{\rm PAH}]_k^{q+}$ according to

$$E_{\rm tot}^{\rm vib}(k-1) = [1 - 1/k]\big[E_{\rm tot}^{\rm vib}(k) - (6/2)k_BT - E_d(k)\big], \qquad (4)$$

where $(6/2)k_BT$ is the average of the sum of the translational and rotational energy of the emitted monomer. Following the evaporation sequence further gives, in total, k coupled differential equations [55]. These are solved for the distribution of daughter cluster ions from a parent cluster of size k, with total internal vibrational energy $E_{\rm tot}^{\rm vib}$, after 0.6 μs, the average time an ion spends in the interaction region before extraction.

In Fig. 4 we show the energy per molecule, as a function of k, required to completely evaporate an anthracene or a coronene cluster of size k. Somewhat arbitrarily, we set the criterium for complete evaporation such that at least 99% of the parent clusters should have evaporated down to the monomer within 0.6 μs. Temperatures required for complete evaporation of the cluster sizes in Fig. 4 lie in the range from a few hundred kelvin up to slightly over 1000 K. This range justifies the approach of Eq. (3) as some intramolecular

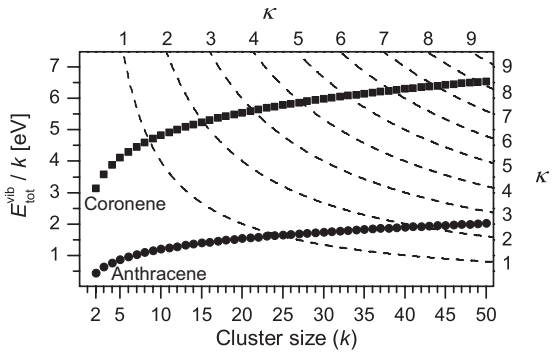

FIG. 4. The total cluster vibrational energy per molecule $E_{\rm tot}^{\rm vib}/k$ required to completely evaporate a cluster of size k of coronene (squares) or anthracene (circles) molecules. Dashed lines mark different κ, an upper boundary for the number of molecules within the cluster that the He^{2+} projectile typically must pass through in order to transfer sufficient energy for complete cluster evaporation. We assume that 40 eV is transferred to the cluster for each constituent molecule hit (see text).

vibrational modes may be inactive at these temperatures [48]. Fig. 4 also clearly shows that more energy is required per molecule to completely evaporate a coronene than an anthracene cluster for a given k. This is because the former have larger dissociation energies E_d and larger numbers of internal vibrational modes and may thus store more energy. Due to the large probability for ionizing He^{2+} projectiles to pass through the plane of an anthracene or a coronene molecule [20] and due to similar local electron densities around the hexagons in anthracene or coronene molecules, we assume the same average excitation energy (40 eV) in both cases. We then estimate how many molecules κ in a cluster that the He^{2+} projectile has to pass through in order to induce sufficient excitation energy for a singly charged cluster, $[{\rm PAH}]_k^+$, to evaporate down to the PAH^+ monomer. The dashed lines in Fig. 4 are curves of $E_{\rm tot}^{\rm vib}/k = 40\kappa/k$ eV for different values of κ. It is thus sufficient for a He^{2+} projectile to pass through only one molecule, $\kappa = 1$, for coronene clusters with $k \leqslant 8$ or anthracene clusters with $k \leqslant 24$ to evaporate completely. A coronene cluster with $k = 24$ will evaporate completely if the projectile passes through $\kappa = 4$ molecules. For $k = 50$ the projectile has to pass through $\kappa = 9$ molecules to completely evaporate a coronene cluster but only $\kappa = 3$ molecules to completely evaporate a $k = 50$ anthracene cluster. Thus, it is reasonable that slightly more of the larger clusters are observed for the coronene clusters because a substantially larger number of the coronene molecules have to be hit for complete cluster evaporation. The general conclusions from the model are not very sensitive to the model parameters. Changing, e.g., A in Eq. (1) by two orders of magnitude changes κ for $k = 50$ by zero and two units for anthracene and coronene clusters, respectively

Low-charge-state ions may be similarly destructive for PAH clusters also at slightly lower projectile velocities v than the ones used here, e.g., those found in stellar winds. The solar wind has two modes, one with $v \simeq 400$ km s^{-1} (35% of the v of the present ion projectiles) and one with $v \simeq 750$ km s^{-1} (66% of the v of the present ion projectiles) at the Earth's orbit [56]. At these v the electronic stopping peaks

at ∼13 and ∼25 eV [20], respectively, and shifts the dashed κ curves in Fig. 4 accordingly. For 13-eV electronic stopping per molecule hit, an ion passing through $\kappa = 1$ molecule is sufficient to completely evaporate $k = 3$ coronene clusters or $k = 8$ anthracene clusters within 0.6 μs. Considering the much longer time scales relevant under astrophysical conditions, we find that it is sufficient for low-charge-state solar wind ions to hit only one or two molecules in $k = 50$ coronene clusters for them to decrease in size within 1 s. However, it should be noted that at such long time scales cooling by evaporation will compete with cooling by infrared emission [57].

IV. RESULTS AND DISCUSSION FOR Xe^{20+} PROJECTILES

A. Coronene cluster targets

Holm *et al.* [21] found that Xe^{20+} ions induce much more fragmentation in the anthracene cluster targets than He^+ ions. This was very unexpected as Xe^{20+} ions most likely remove electrons from any target, including PAH clusters, at much larger distances than He^+ (or He^{2+}) projectiles and should thus induce much less heating. The cluster size-to-charge spectrum due to Xe^{20+} collisions on coronene cluster targets is shown in Fig. 5, and it is dominated strongly by the $C_{24}H_{12}^+$ peak, the main product of the cluster fragmentation processes. Singly charged dimers and trimers are also visible, but peaks due to larger cluster sizes (larger j) are, compared to the results for He^{2+} projectiles (Fig. 3), much weaker and only product clusters up to $j = 15$ may be identified. This fragmentation behavior is qualitatively similar to the one for Xe^{20+} ions colliding with anthracene cluster targets (see Fig. 1 in Ref. [21]) or pyrene or fluoranthene cluster targets [58]. Apparently, the increased number of internal vibrational modes in coronene compared to anthracene does not influence the PAH cluster fragmentation behavior to any greater extent when ionized in collisions with highly charged ions.

B. Multiple ionization of coronene clusters

The simplest version of the classical over-the-barrier model [59] suggests that with Xe^{20+} projectiles the critical distance for electron capture (from the center of the coronene molecule) is four times larger than the molecular radius [22,23]. Thus electronic stopping should be much less important here than for He^{2+}, where close interactions are needed for ionization. We have calculated single and multiple IEs for different coronene cluster sizes using DFT with the M06-2X functional and the 6-31+G(d,p) basis set as implemented in the GAUSSIAN09 program suite [53]. The M06-2X is a hybrid meta exchange-correlation functional suitable for noncovalent interactions [60], as is important for neutral clusters, and it has shown good agreement with high-level *ab initio* calculations for the coronene dimer [42]. We performed our calculations as single point calculations with twisted sandwich (TS, see inset in Fig. 6, left panel) [39] stacks constructed from the optimized monomer structure of Zhao and Truhlar [39]. Here we assumed the stacks to grow with the same intermolecular distance, 3.4 Å, as in the optimized TS *dimer* structure [39]. The validity of this approach was tested by calculating the IEs of the *optimized* TS dimer of Zhao and Truhlar [39], their parallel-displaced-1 (PD-1) dimer configuration, and our simplified approach with nonrelaxed molecules in the TS dimer configuration. Our calculated IEs for these three configurations differ by less than 0.05 eV, indicating that the IEs are sensitive neither to the manner in which the coronene molecules are stacked nor to the precise structures (relaxed or non-relaxed) of the individual molecules in the coronene cluster.

In Fig. 6, left panel, we show our calculated first and second IEs for coronene clusters as functions of cluster size, k. These values compare well with experimental data ([29] and references therein) and other calculations [44]. In the right panel in Fig. 6 we show our calculated IEs as functions of the initial charge states for different cluster sizes k together with linear fits to the IEs for each k. In addition, experimental data [29] for $k = 1$ are shown. The fits are based on the classical electrostatic expression for a conducting object [61],

$$I_k^{q+1} = W_k + \frac{e(q + 1/2)}{C_k}. \tag{5}$$

Here I_k^{q+1} is the $(q + 1)$th IE of a cluster of size k, where q is the cluster charge state, W_k is the work function (in eV), e is the elementary charge, and C_k is the capacitance (in farad). In Table I we list the numerical (fitted) values for W_k and C_k. For the clusters ($k > 1$) the IEs follow linear trends and the capacitance changes with k such that $\triangle C_{k\to k+1} = C_{k+1} - C_k$ is constant within the present uncertainties. For single stacks of coronene molecules the results may thus be summarized as

$$I_{k>1}^{q+1} = 5.457 + \frac{q + 1/2}{0.046k + 0.237}\ \text{eV}. \tag{6}$$

A correlation plot between the IEs of Eq. (6) and the DFT IEs themselves is shown in the inset in the right panel of Fig. 6.

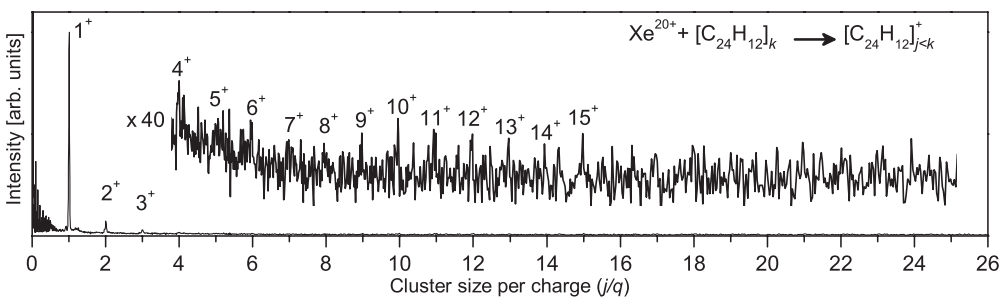

FIG. 5. Size-to-charge spectrum for ionized and fragmented coronene cluster targets following collisions with Xe^{20+} ions, with an enlarged view for $j \geqslant 4$.

TABLE I. The work function W_k and the capacitance divided by the elementary charge e, C_k/e, for the fitted IE values [Eq. (5)]. The resulting IEs are shown as solid lines in the right panel of Fig. 6.

k	W_k [eV]	C_k/e [F/C]
1	5.66 ± 0.45	0.27 ± 0.01
2	5.48 ± 0.21	0.33 ± 0.01
3	5.44 ± 0.17	0.38 ± 0.01
4	5.45 ± 0.18	0.42 ± 0.01
5	5.46 ± 0.18	0.47 ± 0.02

The slopes of the $I_{k>1}^{q+1}$ as functions of q decrease with increasing k, which means not only that larger clusters are more easily ionized but also that the cross section for multiple electron capture increases strongly in relation to the single-electron-capture cross section. A similar effect has been observed and accounted for by means of an electrostatic model [62] applied to experimental results for large clusters of fullerenes [63,64] and in particular to multiply ionized C_{60} dimers [64,65]. The dashed lines in Fig. 6 indicate the slopes for the IEs for $k = 10$, 25, and 50, obtained with Eq. (6). These highlight the trend of more efficient multiple ionizations with increasing cluster size. It should be noted, however, that Eq. (6) may not be as accurate for larger cluster sizes where three-dimensional geometries become more favorable compared to the single-stack configuration [43].

Multiple-electron removal leads to a Coulomb explosion, which effectively destroys larger clusters. Such events also induce strong heating of the individual molecules as large parts of the Coulomb potential energies are converted to internal vibrational energy in the fragment ions (see, e.g., Fig. 6 in Ref. [64]). This explains the internally very hot fragmentation products following Xe^{20+} collisions observed here for coronene cluster targets and that have been observed earlier for anthracene cluster targets [21] as well as for clusters of the PAH molecules pyrene and fluoranthene [58]. Most likely, this also means that PAH clusters would be multiply ionized by the more highly charged of the solar wind ions, such as C^{6+}, O^{6+}, Si^{9+}, and Fe^{10+} [66], which then would lead to prompt fragmentations.

V. SUMMARY AND CONCLUSIONS

In this work we have reported an experimental investigation of the ionization and the fragmentation of singly and multiply charged pure clusters of k PAH molecules of anthracene, $C_{14}H_{10}$, or coronene, $C_{24}H_{12}$. Both types of clusters were ionized and excited in 22.5-keV He^{2+} collisions and for the coronene clusters also in 360-keV Xe^{20+} collisions. In all cases, the clusters fragment promptly, i.e., on submicrosecond time scales with very high probabilities. All fragment distributions are strongly dominated by singly charged monomers, $C_{14}H_{10}^+$ or $C_{24}H_{12}^+$, and all fragment distributions exhibit strongly decreasing intensities as functions of increasing product cluster size j.

For the He^{2+} collisions the clusters are moderately charged and internally rather strongly excited in small impact parameter collisions with large energy transfers dominated by electronic stopping processes. This yields long series of $C_{14}H_{10}$ or $C_{24}H_{12}$ monomer evaporations through which the daughter ions are slowly cooled, leaving the final monomer daughter ions relatively cold, such that further fragmentation becomes unlikely. By means of a simple monomer evaporation model it is possible to account for the observed long evaporation sequences.

With the Xe^{20+} collisions, the fragmentation mechanism is most likely different as here several electrons are efficiently removed at large distances where electronic stopping is negligible, and thus there will be little initial heating of the clusters. Such multiple ionization processes are followed by Coulomb explosions of the weakly bound clusters, inducing strong

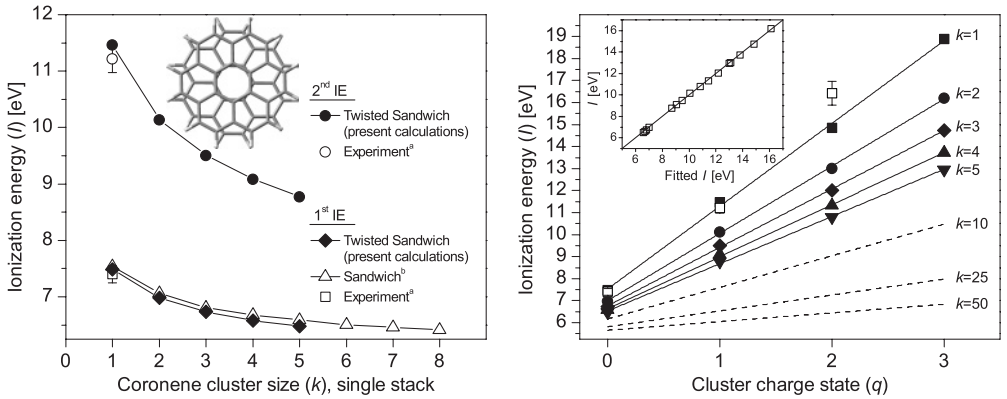

FIG. 6. (left) Calculated first and second ionization energies (IEs) as functions of cluster size k. Comparisons with experiments and other calculations are as follows: a, electron impact ionization [29] and b, calculations for sandwich (S) configurations using a density functional theory based tight-binding approximation where charge delocalization is treated with a configuration interaction-like scheme (DFTB+CI) [44]. The inset shows a top view of the twisted sandwich (TS) configuration used in the present calculations for the coronene dimer. (right) Calculated IEs as functions of charge state q before ionization for different cluster sizes, with linear fits to each set of the data. The inset shows a correlation plot between IEs obtained from the linear fits to the calculated DFT values [Eq. (6)] and the calculated DFT values themselves. A line marking the one-to-one relation between these two sets of values is plotted along the diagonal. The dashed lines for $k = 10$, $k = 25$, and $k = 50$ are obtained using Eq. (6) and represent extrapolations to larger single stacks, though larger clusters may have more complex geometries. The open squares are experimental results [29].

internal heating in the individual molecules and subsequent fragmentations down to the monomer ions. These monomer ions are also much hotter than in the case of the He^{2+} collisions as substantial parts of the Coulomb potential energy may be converted to the internal vibrational modes in the individual molecules. Indeed, we observe very strong fragmentation of the $C_{24}H_{12}^{+}$ products following Xe^{20+} collisions. The essential aspect here is that multiple electron removal becomes very strong in relation to pure single-electron capture for PAH clusters. The reason for this is lowered multiple ionization energies, as shown by our calculated and modeled values, which are parameterized with a common work function (independent of k) and a capacitance that scales with cluster size k.

From the present study we conclude that interactions between PAH clusters and stellar wind ions with velocities from 400 to 750 km s^{-1} would lead to rapid disintegration of the clusters. The mechanism is, however, different depending on the charge state of the ions: low-charge-state ions transfer heat directly in the collisions, and higher-charge-state ions predominantly remove more than one electron, leading to Coulomb explosions. The present study indicates that only very large clusters consisting of larger PAH molecules may survive as somewhat smaller clusters on long time scales following ionization in *single* interactions with light solar wind ions.

No fusion reactions between different molecules in PAH clusters, similar to what has been found for fullerene clusters exposed to similar ion collisions [67], could be identified. Furthermore, no magic cluster sizes were observed, which most likely relates to the present rather high internal cluster excitation energies.

ACKNOWLEDGMENTS

These studies were performed at the ARIBE facility, part of the distributed LEIF infrastructure. Financial support received from the ITS-LEIF project (Grant No. RII3-026015), the Swedish Research Council, and the Danish Council for Independent Research/Natural Science is gratefully acknowledged. The authors thank F. Noury and L. Maunoury for technical support.

[1] M. Frenklach, PhysChemChemPhys. **4**, 2028 (2002).
[2] W. Wilcke, Geoderma **141**, 157 (2007).
[3] C. Bosetti, P. Boffetta, and C. La Vecchia, Ann. Oncol. **18**, 431 (2007).
[4] A. G. G. M. Tielens, Annu. Rev. Astron. Astrophys. **46**, 289 (2008).
[5] T. S. Totton, D. Chakrabarti, A. J. Misquitta, M. Sander, D. J. Wales, and M. Kraft, Combust. Flame **157**, 909 (2010).
[6] Á. J. Pérez-Jiménez and J. C. Sancho-García, J. Am. Chem. Soc. **131**, 14857 (2009).
[7] M. Rapacioli, C. Joblin, and P. Boissel, Astron. Astrophys. **429**, 193 (2005).
[8] O. Berné, C. Joblin, Y. Deville, J. D. Smith, M. Rapacioli, J. P. Bernard, J. Thomas, W. Reach, and A. Abergel, Astron. Astrophys. **469**, 575 (2007).
[9] Y. Gotkis, M. Oleinikova, M. Naor, and C. Lifshitz, J. Phys. Chem. **97**, 12282 (1993).
[10] H. W. Jochims, E. Rühl, H. Baumgärtel, S. Tobita, and S. Leach, Astrophys. J. **420**, 307 (1994).
[11] S. P. Ekern, A. G. Marshall, J. Szczepanski, and M. Vala, Astrophys. J. **488**, L39 (1997).
[12] S. P. Ekern, A. G. Marshall, J. Szczepanski, and M. Vala, J. Phys. Chem. A **102**, 3498 (1998).
[13] Y. Ling and C. Lifshitz, J. Phys. Chem. A **102**, 708 (1998).
[14] J. Oomens, A. J. A. van Roij, G. Meijer, and G. von Helden, Astrophys. J. **542**, 404 (2000).
[15] L. Robson, K. W. D. Ledingham, A. D. Tasker, P. McKenna, T. McCanny, C. Kosmidis, D. A. Jaroszynski, D. R. Jones, R. C. Issac, and S. Jamieson, Chem. Phys. Lett. **360**, 382 (2002).
[16] L. Robson, A. D. Tasker, K. W. D. Ledingham, P. McKenna, T. McCanny, C. Kosmidis, P. Tzallas, D. A. Jaroszynski, and D. R. Jones, Int. J. Mass Spectrom. **220**, 69 (2002).
[17] M. Murakami, R. Mizoguchi, Y. Shimada, T. Yatsuhashi, and N. Nakashima, Chem. Phys. Lett. **403**, 238 (2005).
[18] X. M. Wang, H. Becker, A. C. Hopkinson, R. E. March, L. T. Scott, and D. K. Bohme, Int. J. Mass Spectrom. Ion Processes **161**, 69 (1997).
[19] R. Arakawa, M. Kobayashi, and T. Nishimura, J. Mass Spectrom. **35**, 178 (2000).
[20] J. Postma, S. Bari, R. Hoekstra, A. G. G. M. Tielens, and T. Schlatholter, Astrophys. J. **708**, 435 (2010).
[21] A. I. S. Holm *et al.*, Phys. Rev. Lett. **105**, 213401 (2010).
[22] A. Ławicki *et al.*, Phys. Rev. A **83**, 022704 (2011).
[23] A. I. S. Holm, H. A. B. Johansson, H. Cederquist, and H. Zettergren, J. Chem. Phys. **134**, 044301 (2011).
[24] D. Biermann and W. Schmidt, J. Am. Chem. Soc. **102**, 3163 (1980).
[25] J. W. Hager and S. C. Wallace, Anal. Chem. **60**, 5 (1988).
[26] E. Clar, J. M. Robertson, R. Schlögl, and W. Schmidt, J. Am. Chem. Soc. **103**, 1320 (1981).
[27] S. Tobita, S. Leach, H. W. Jochims, E. Rühl, E. Illenberger, and H. Baumgärtel, Can. J. Phys. **72**, 1060 (1994).
[28] D. Schröder, J. Loos, H. Schwarz, R. Thissen, D. V. Preda, L. T. Scott, D. Caraiman, M. V. Frach, and D. K. Böhme, Helv. Chim. Acta **84**, 1625 (2001).
[29] S. Denifl, B. Sonnweber, J. Mack, L. T. Scott, P. Scheier, K. Becker, and T. D. Märk, Int. J. Mass Spectrom. **249**, 353 (2006).
[30] M. S. Deleuze, L. Claes, E. S. Kryachko, and J. P. François, J. Chem. Phys. **119**, 3106 (2003).
[31] Y. L. Xiao and D. E. Williams, Chem. Phys. Lett. **215**, 17 (1993).
[32] R. P. White, J. A. Niesse, and H. R. Mayne, J. Chem. Phys. **108**, 2208 (1998).
[33] B. Bouvier, V. Brenner, P. Millié, and J. M. Soudan, J. Phys. Chem. A **106**, 10326 (2002).
[34] F. Piuzzi, I. Dimicoli, M. Mons, P. Millie, V. Brenner, Q. Zhao, B. Soep, and A. Tramer, Chem. Phys. **275**, 123 (2002).
[35] D. W. J. Cruickshank, Acta Crystallogr. **9**, 915 (1956).
[36] S. D. Chakarova-Käck, A. Vojvodic, J. Kleis, P. Hyldgaard, and E. Schröder, New J. Phys. **12**, 013017 (2010).

[37] T. S. Totton, A. J. Misquitta, and M. Kraft, J. Chem. Theory Comput. **6**, 683 (2010).
[38] O. I. Obolensky, V. V. Semenikhina, A. V. Solov'yov, and W. Greiner, Int. J. Quantum Chem. **107**, 1335 (2007).
[39] Y. Zhao and D. G. Truhlar, J. Phys. Chem. C **112**, 4061 (2008).
[40] M. Rapacioli, F. Spiegelman, D. Talbi, T. Mineva, A. Goursot, T. Heine, and G. Seifert, J. Chem. Phys. **130**, 244304 (2009).
[41] R. Podeszwa, J. Chem. Phys. **132**, 044704 (2010).
[42] T. Janowski, A. R. Ford, and P. Pulay, Mol. Phys. **108**, 249 (2010).
[43] M. Rapacioli, F. Calvo, F. Spiegelman, C. Joblin, and D. J. Wales, J. Phys. Chem. A **109**, 2487 (2005).
[44] M. Rapacioli and F. Spiegelman, Eur. Phys. J. D **52**, 55 (2009).
[45] T. Chakraborty and E. C. Lim, J. Phys. Chem. **97**, 11151 (1993).
[46] J. K. Song, N. K. Lee, J. H. Kim, S. Y. Han, and S. K. Kim, J. Chem. Phys. **119**, 3071 (2003).
[47] P. Bréchignac, M. Schmidt, A. Masson, T. Pino, P. Parneix, and C. Bréchignac, Astron. Astrophys. **442**, 239 (2005).
[48] M. Schmidt, A. Masson, and C. Bréchignac, Int. J. Mass Spectrom. **252**, 173 (2006).
[49] T. Bergen *et al*., Rev. Sci. Instrum. **70**, 3244 (1999).
[50] F. Chandezon, B. Huber, and C. Ristori, Rev. Sci. Instrum. **65**, 3344 (1994).
[51] N. R. Daly, Rev. Sci. Instrum. **31**, 720 (1960).
[52] J. Maul, T. Berg, E. Marosits, G. Schönhense, and G. Huber, Phys. Rev. B **74**, 161406 (2006).
[53] M. J. Frisch, G. W. Trucks, H. B. Schlegel, G. E. Scuseria, M. A. Robb, J. R. Cheeseman, G. Scalmani, V. Barone, B. Mennucci, G. A. Petersson, H. Nakatsuji, M. Caricato, X. Li, H. P. Hratchian, A. F. Izmaylov, J. Bloino, G. Zheng, J. L. Sonnenberg, M. Hada, M. Ehara, K. Toyota, R. Fukuda, J. Hasegawa, M. Ishida, T. Nakajima, Y. Honda, O. Kitao, H. Nakai, T. Vreven, J. A. Montgomery Jr., J. E. Peralta, F. Ogliaro, M. Bearpark, J. J. Heyd, E. Brothers, K. N. Kudin, V. N. Staroverov, R. Kobayashi, J. Normand, K. Raghavachari, A. Rendell, J. C. Burant, S. S. Iyengar, J. Tomasi, M. Cossi, N. Rega, J. M. Millam, M. Klene, J. E. Knox, J. B. Cross, V. Bakken, C. Adamo, J. Jaramillo, R. Gomperts, R. E. Stratmann, O. Yazyev, A. J. Austin, R. Cammi, C. Pomelli, J. W. Ochterski, R. L. Martin, K. Morokuma, V. G. Zakrzewski, G. A. Voth, P. Salvador, J. J. Dannenberg, S. Dapprich, A. D. Daniels, Ö. Farkas, J. B. Foresman, J. V. Ortiz, J. Cioslowski, and D. J. Fox, GAUSSIAN 09 revision A.2, Gaussian, Inc. Wallingford, CT, 2009.
[54] M. P. Andersson and P. Uvdal, J. Phys. Chem. A **109**, 2937 (2005).
[55] N. Haag, B. Liu, S. B. Nielsen, H. Zettergren, P. Hvelplund, B. Manil, B. A. Huber, H. A. B. Johansson, H. T. Schmidt, and H. Cederquist, J. Phys. Conf. Ser. **194**, 012053 (2009).
[56] *Cosmic Winds and the Heliosphere*, edited by J. R. Jokipii, S. P. Sonett, and M. S. Giampapa (University of Arizona Press, Tucson, 1997).
[57] M. Rapacioli, F. Calvo, C. Joblin, P. Parneix, D. Toublanc, and F. Spiegelman, Astron. Astrophys. **460**, 519 (2006).
[58] F. Seitz *et al*., J. Chem. Phys. **135**, 064302 (2011).
[59] A. Bárány, G. Astner, H. Cederquist, H. Danared, S. Huldt, P. Hvelplund, A. Johnson, H. Knudsen, L. Liljeby, and K. G. Rensfelt, Nucl. Instrum. Methods Phys. Res., Sect. B **9**, 397 (1985).
[60] Y. Zhao and D. G. Truhlar, Theor. Chem. Acc. **120**, 215 (2008).
[61] F. T. Smith, J. Chem. Phys. **34**, 793 (1961).
[62] H. Zettergren, H. T. Schmidt, H. Cederquist, J. Jensen, S. Tomita, P. Hvelplund, H. Lebius, and B. A. Huber, Phys. Rev. A **66**, 032710 (2002).
[63] B. Manil, L. Maunoury, B. A. Huber, J. Jensen, H. T. Schmidt, H. Zettergren, H. Cederquist, S. Tomita, and P. Hvelplund, Phys. Rev. Lett. **91**, 215504 (2003).
[64] H. Zettergren, H. T. Schmidt, P. Reinhed, H. Cederquist, J. Jensen, P. Hvelplund, S. Tomita, B. Manil, J. Rangama, and B. A. Huber, J. Chem. Phys. **126**, 224303 (2007).
[65] H. Zettergren, H. T. Schmidt, P. Reinhed, H. Cederquist, J. Jensen, P. Hvelplund, S. Tomita, B. Manil, J. Rangama, and B. A. Huber, Phys. Rev. A **75**, 051201 (2007).
[66] J. R. Gruesbeck, S. T. Lepri, T. H. Zurbuchen, and S. K. Antiochos, Astrophys. J. **730**, 103 (2011).
[67] H. Zettergren *et al*., J. Chem. Phys. **133**, 104301 (2010).